

Dynamical taxonomy of the coupled solar radiation pressure and oblateness problem and analytical deorbiting configurations

Ioannis Gkolias · Elisa Maria Alessi ·
Camilla Colombo

Received: date / Accepted: date

Abstract Recent works demonstrated that the dynamics caused by the planetary oblateness coupled with the solar radiation pressure can be described through a model based on singly-averaged equations of motion. The coupled perturbations affect the evolution of the eccentricity, inclination and orientation of the orbit with respect to the Sun–Earth line. Resonant interactions lead to non-trivial orbital evolution that can be exploited in mission design. Moreover, the dynamics in the vicinity of each resonance can be analytically described by a resonant model that provides the location of the central and hyperbolic invariant manifolds which drive the phase space evolution. The classical tools of the dynamical systems theory can be applied to perform a preliminary mission analysis for practical applications. On this basis, in this work we provide a detailed derivation of the resonant dynamics, also in non-singular variables, and discuss its properties, by studying the main bifurcation phenomena associated to each resonance. Last, the analytical model will provide a simple analytical expression to obtain the area-to-mass ratio required for a satellite to deorbit from a given altitude in a feasible timescale.

Keywords solar radiation pressure · oblateness · averaged dynamics · equilibrium points · bifurcation diagrams · deorbiting

I. Gkolias

Department of Aerospace Science and Technology, Politecnico di Milano, Via la Masa 34, 20156 Milan, Italy E-mail: ioannis.gkolias@polimi.it

E. M. Alessi

Istituto di Matematica Applicata e Tecnologie Informatiche "Enrico Magenes", Consiglio Nazionale delle Ricerche, Via Alfonso Corti 12, 20133 Milano, Italy

Istituto di Fisica Applicata "Nello Carrara", Consiglio Nazionale delle Ricerche, Via Madonna del Piano 10, 50019 Sesto Fiorentino (FI), Italy E-mail: elisamaria.alessi@cnr.it

C. Colombo

Department of Aerospace Science and Technology, Politecnico di Milano, Via la Masa 34, 20156 Milan, Italy E-mail: camilla.colombo@polimi.it

1 Introduction

The effect of the Solar Radiation Pressure (SRP) on Earth satellites was recognised since the first space flights. The orbital evolution of Vanguard I [16] and the Echo balloons [20] was found to be significantly influenced by SRP, and singly-averaged equations were used to study the motion [15]. Treated as a perturbation problem, the singly-averaged contribution of SRP is integrable and analytical solutions can be obtained [14, 17, 19]. Nevertheless, when coupled with the effect of Earth's oblateness J_2 the system becomes a 2.5 Degrees-of-Freedom (DoF). An analytical insight can be recovered when treating locally the semi-secular SRP resonances. Namely, the singly-averaged perturbing function can be decomposed in six distinct terms [8], each of them dominating in a particular range of orbital elements. The dynamics arising by combining each of the harmonics with the secular evolution due to J_2 can be reduced to a 1 DoF *resonant* model [10, 12, 2].

The derivation of the six different resonant models in the three-dimensional case and their effect on the long-term evolution of resident space objects has been recently discussed in the literature [2, 1]. In this work, we re-derive the resonant models in the Hamiltonian framework, providing also a non-singular representation of the resonant dynamics. We exploit the information of the analytical model in [1] to obtain further insight in the resonant structures. We employ the equations for computing the equilibria for each resonance and compute the number and their stability for each set of the dynamical parameters of the system. This allows us to construct bifurcations diagrams which give the main transitions in the phase space. Particular focus is given to the structure of the phase space about the vicinity of each SRP resonance. The effect of the engineering parameter, the spacecraft area-to-mass ratio, is also discussed.

Using the phase space portraits, useful information for mission design concepts is retrieved via the tools of dynamical system theory. In particular, a rigorous procedure to obtain deorbiting conditions along the resonances is presented. As for the planar case [12], we show how the deorbiting can occur.

The paper is organised in the following way: in Sec. 2 the basic force model is recovered in its singly-averaged formulation, in Sec. 3 we discuss the analytical description in the vicinity of SRP resonances, in Sec. 4 we provide a phase space analysis based on the main bifurcations associated to each resonance, in Sec. 5 we demonstrate the use of the models to analytically obtain feasible deorbiting configurations, and in Sec. 6 we present our conclusions.

2 Model derivation

Let us assume that a spacecraft moves under the effect of a planet's gravitational monopole, the planetary oblateness and the solar radiation pressure. Moreover, we assume that the sun-rays are always perpendicular to the surface of the satellite (cannonball model), that the effect of the planetary albedo

is negligible, that the solar flux is constant at 1 AU and that the satellite is entirely in sunlight. Under these assumptions, SRP is modelled as a constant force in the direction of the Earth-Sun line, and it can be derived from a potential function. The dynamics of the satellite in a geocentric equatorial inertial frame can be modelled by the Hamiltonian

$$\mathcal{H} = \mathcal{H}_{kep} + \mathcal{H}_{J_2} + \mathcal{H}_{SRP}.$$

The Keplerian part \mathcal{H}_{kep} reads

$$\mathcal{H}_{kep} = \frac{v^2}{2} - \frac{\mu}{r},$$

where μ is the gravitational parameter of the Earth, and r, v are the geocentric distance and velocity of the satellite.

The Earth's oblateness effect is modelled as

$$\mathcal{H}_{J_2} = \frac{\mathcal{C}_{J_2} (3 \sin^2 \phi - 1)}{2r^3},$$

where $\mathcal{C}_{J_2} = \mu R_\oplus^2 J_2$ with J_2 the oblateness parameter and ϕ the geographic latitude of the satellite. The sine of the latitude is expressed in terms of the orbital elements of the satellite via

$$\sin \phi = \frac{z}{r},$$

and

$$z = (0, 0, 1) \cdot R_3(-\Omega)R_1(-i)R_3(-\lambda) \cdot (r, 0, 0)^T,$$

where i is the inclination, Ω the Right Ascension of the Ascending Node (RAAN), $\lambda = \omega + f$ the longitude, ω the argument of perigee and f the true anomaly of the satellite. The rotation matrices $R_1(u), R_3(u)$ are

$$R_1(u) = \begin{pmatrix} 1 & 0 & 0 \\ 0 & \cos u & \sin u \\ 0 & -\sin u & \cos u \end{pmatrix}, \quad R_3(u) = \begin{pmatrix} \cos u & \sin u & 0 \\ -\sin u & \cos u & 0 \\ 0 & 0 & 1 \end{pmatrix}. \quad (1)$$

The solar radiation pressure contribution is given by

$$\mathcal{H}_{SRP} = \mathcal{C}_{SRP} X,$$

where $\mathcal{C}_{SRP} = P_\odot c_R \frac{A}{m}$, P_\odot being the SRP constant at 1 AU , c_R the reflectivity coefficient and $\frac{A}{m}$ the area-to-mass ratio of the satellite. X is the coordinate of the satellite in an Earth-centred system with the X-axis pointed towards the Sun (see Fig. 1): in terms of the orbital elements of the satellite it reads

$$X = (1, 0, 0) \cdot R_3(\lambda_\odot)R_1(\varepsilon)R_3(-\Omega)R_1(-i)R_3(-\theta) \cdot (r, 0, 0)^T,$$

with λ_\odot the ecliptic longitude of the Sun and ε the obliquity of the ecliptic.

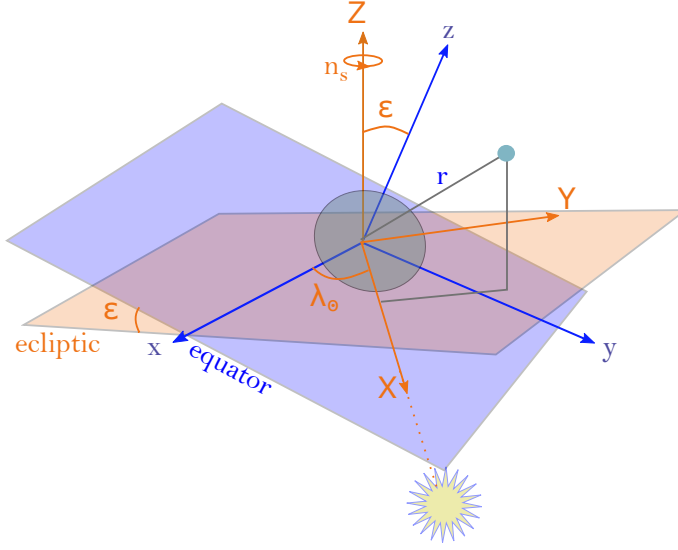


Fig. 1 Schematic description of an equatorial inertial and an ecliptic rotating reference frames. The solar radiation pressure is modelled as a constant force in the direction of the Sun.

Both \mathcal{H}_{J_2} and \mathcal{H}_{SRP} are considerable smaller than \mathcal{H}_{kep} and can be treated as perturbations of the two-body problem

$$\mathcal{H} = \mathcal{H}_{kep} + \mathcal{H}_{per},$$

where $\mathcal{H}_{per} = \mathcal{H}_{J_2} + \mathcal{H}_{SRP}$. Employing a Hori-Deprit approach [7,6], the homological equation up to the first order of the normalisation process reads:

$$n \frac{\partial W_1}{\partial M} = \mathcal{H}_{per} - \bar{\mathcal{H}}_{per},$$

where n is the mean motion of the satellite, W_1 is the generating function and

$$\bar{\mathcal{H}}_{per} = \frac{1}{2\pi} \int_0^{2\pi} \mathcal{H}_{per} dM, \quad (2)$$

is the first-order normalized Hamiltonian. The integrals in Eq. (2) can be carried out in closed form for both the J_2 and SRP contributions. In the case of J_2 we use the differential relationship $dM = \frac{r^2}{a\sqrt{1-e^2}} df$ along with $r = a \frac{1-e^2}{1+e \cos f}$ to obtain the classical result

$$\bar{\mathcal{H}}_{J_2} = \frac{\mathcal{C}_{J_2}(3c_i^2 - 1)}{4a^3(1 - e^2)^{3/2}}, \quad (3)$$

where $c_i = \cos i$. For SRP we express the integral with respect to the eccentric anomaly E using the relations $r \sin f = a\sqrt{1 - e^2} \sin E$, $r \cos f = a(\cos E - e)$, $r = a(1 - e \cos E)$ and $dM = \frac{r}{a} dE$.

The averaged model is then [10, 12, 2]

$$\bar{\mathcal{H}}_{SRP} = -\frac{3}{2}ae\mathcal{C}_{SRP} \sum_{j=1}^6 \mathcal{T}_j \cos \psi_j, \quad (4)$$

with

j	\mathcal{T}_j	$\cos \psi_j$	(n_1, n_2, n_3)
1	$\frac{1}{4}(c_\varepsilon + 1)(c_i + 1)$	$\cos(\omega + \Omega - \lambda_\odot)$	$(\pm 1, \pm 1, \mp 1)$
2	$-\frac{1}{4}(c_\varepsilon + 1)(c_i - 1)$	$\cos(-\omega + \Omega - \lambda_\odot)$	$(\mp 1, \pm 1, \mp 1)$
3	$\frac{1}{2}s_i s_\varepsilon$	$\cos(\omega - \lambda_\odot)$	$(\pm 1, 0, \mp 1)$
4	$-\frac{1}{2}s_i s_\varepsilon$	$\cos(\omega + \lambda_\odot)$	$(\pm 1, 0, \pm 1)$
5	$-\frac{1}{4}(c_\varepsilon - 1)(c_i + 1)$	$\cos(\omega + \Omega + \lambda_\odot)$	$(\pm 1, \pm 1, \pm 1)$
6	$\frac{1}{4}(c_\varepsilon - 1)(c_i - 1)$	$\cos(-\omega + \Omega + \lambda_\odot)$	$(\mp 1, \pm 1, \pm 1)$

(5)

where $c_i, s_i, c_\varepsilon, s_\varepsilon$ are the cosine and sine of the inclination i and the obliquity of the ecliptic ε , respectively. The model consists of 6 distinct harmonics describing the semi-secular evolution of the system, all of them containing the ecliptic longitude of the Sun λ_\odot . A second averaging of over Sun's mean motion results in a null Hamiltonian, that is, the SRP perturbation does not give rise to secular effects. Moreover, we should mention that the Hamiltonian Eq. (4) is integrable, and an analytical solution is obtained using an ecliptic rotating frame [14].

The singly-averaged model of the coupled Earth's oblateness and solar radiation pressure effects reads

$$\bar{\mathcal{H}} = \bar{\mathcal{H}}_{J_2} + \bar{\mathcal{H}}_{SRP}.$$

The Hamiltonian can be expressed in terms of the canonical Delaunay elements (L, G, H, l, g, h) such that

$$\begin{aligned} L &= \sqrt{\mu a}, & l &= M, \\ G &= L\sqrt{1 - e^2}, & g &= \omega, \\ H &= G \cos i, & h &= \Omega, \end{aligned} \quad (6)$$

to obtain

$$\bar{\mathcal{H}} = \frac{\mathcal{C}_{J_2}\mu^3(G^2 - 3H^2)}{4G^5L^3} - \frac{3\mathcal{C}_{SRP}\sqrt{1 - \frac{G^2}{L^2}}L^2}{2\mu} \sum_{j=1}^6 \mathcal{T}_j \cos \psi_j, \quad (7)$$

where for the coefficients \mathcal{T}_j we use the relationships $c_i = H/G, s_i = \sqrt{1 - \frac{H^2}{G^2}}$.

Due to the averaging process, Eq. (7) does not depend on the mean anomaly $M = l$ and thus the Delaunay action L , as well as the semi-major axis, are constant. The system has two Degrees-of-Freedom (DoF) and an explicit time

dependence through $\lambda_\odot(t) = \lambda_{\odot,0} + n_s t$, where n_s is the frequency corresponding to Earth's orbital period of 1 year. Considering an extended phase-space, a dummy action I_s with frequency n_s is added to the Hamiltonian

$$\bar{\mathcal{H}} = \frac{\mathcal{C}_{J_2}\mu^3(G^2 - 3H^2)}{4G^5L^3} - \frac{3\mathcal{C}_{SRP}\sqrt{1 - \frac{G^2}{L^2}}L^2}{2\mu} \sum_{j=1}^6 \mathcal{T}_j \cos \psi_j + n_s I_s,$$

which yields a three DoF autonomous system.

3 Resonances

We are now interested in studying the resonance phenomena occurring in the coupled system. A resonance is occurring when the following commensurability holds:

$$n_1 \dot{g} + n_2 \dot{h} + n_3 \dot{\lambda}_\odot \approx 0 \quad (8)$$

where $\dot{g} = \partial \bar{\mathcal{H}} / \partial G$, $\dot{h} = \partial \bar{\mathcal{H}} / \partial H$ and $\dot{\lambda}_\odot = \partial \bar{\mathcal{H}} / \partial I_s$. The integer coefficients n_1, n_2, n_3 can take the values of the 6 combinations associated to the harmonics appearing in Eq. (5). As a first approximation, the angular frequencies can be computed by taking into account only the H_{J_2} part of the Hamiltonian, namely,

$$\begin{aligned} \dot{g}_{J_2} &= \frac{\partial \bar{\mathcal{H}}}{\partial G} = -\frac{3(G^2 - 5H^2)\mathcal{C}_{J_2}\mu^3}{4G^6L^3} = -\frac{3}{2} \frac{J_2 R_\oplus^2 n}{a^2(1 - e^2)^2} \cos i, \\ \dot{h}_{J_2} &= \frac{\partial \bar{\mathcal{H}}}{\partial H} = -\frac{3H\mathcal{C}_{J_2}\mu^3}{2G^5L^3} = \frac{3}{4} \frac{J_2 R_\oplus^2 n}{a^2(1 - e^2)^2} (5 \cos^2 i - 1), \\ \dot{\lambda}_\odot &= \frac{\partial \bar{\mathcal{H}}}{\partial I_s} = n_s. \end{aligned} \quad (9)$$

Substituting Eq. (9) in Eq. (8), we can derive an approximation of the loci in action-space of the center of each resonance [5,2]. In the vicinity of each resonance, the associate harmonic is slow and is dominating the dynamics. Assuming an isolated resonance approximation, the system can be described locally from the Hamiltonian

$$\mathcal{H}_{\psi_j} = \frac{\mathcal{C}_{J_2}\mu^3(G^2 - 3H^2)}{4G^5L^3} - \frac{3\mathcal{C}_{SRP}\sqrt{1 - \frac{G^2}{L^2}}L^2}{2\mu} \mathcal{T}_j \cos \psi_j + n_s I_s. \quad (10)$$

For each resonance ψ_j (with $j = 1 \dots 6$) we introduce a resonant set of variables (Ψ, ψ) via a unimodular transformation of the Delaunay elements

$$\begin{aligned} \Psi &= \frac{G}{n_1}, & \psi &= n_1 g + n_2 h + n_3 \lambda_\odot, \\ \Pi &= -n_2 G + n_1 H, & \pi &= \frac{h}{n_1}, \\ K &= I_s - \frac{n_3 G}{n_1}, & \kappa &= \lambda_\odot. \end{aligned} \quad (11)$$

which brings the Hamiltonian to a 1-DoF form of

$$H_{\psi_j} = H_{\psi_j, J_2}(\Psi; L, \Pi) + H_{\psi_j, SRP}(\Psi, \psi; L, \Pi) + n_s(n_3\Psi + K),$$

where the part associated with J_2 is

$$\mathcal{H}_{\psi_j, J_2}(\Psi; L, \Pi) = \frac{C_{J_2}\mu^3 (n_1^4\Psi^2 - 3(\Pi + n_1n_2\Psi)^2)}{n_1^7 4L^3\Psi^5}, \quad (12)$$

and the one due to SRP is

$$\mathcal{H}_{\psi_j, SRP}(\Psi, \psi; L, \Pi) = -\frac{3C_{SRP}}{2\mu}L^2\sqrt{1 - \frac{n_1^2\Psi^2}{L^2}}\mathcal{T}_j \cos \psi, \quad (13)$$

while the coefficients \mathcal{T}_j are expressed in terms of the new variables using the equations $c_i = \frac{n_1n_2\Psi + \Pi}{n_2^2\Psi}$ and $s_i = \sqrt{1 - c_i^2}$.

Due to the resonant transformation both π and κ are ignorable, therefore, Π and K are constants and the term n_sK can be dropped from the Hamiltonian. The action variable Π is a resonant integral of the system; its value is dictated from the initial conditions and remains constant during the orbital evolution. Expressed in orbital elements

$$\Pi = \sqrt{\mu a} \sqrt{1 - e^2} (-n_2 + n_1 \cos i) \quad (14)$$

represents coupled oscillations in the eccentricity and inclination of the orbit, in a similar fashion to the Lidov-Kozai constant in the third-body gravitational perturbations [11, 9]. Note that Π corresponds to Λ in [1]. The formulation provided here is equivalent to the one given in the past paper, but n_1 and n_2 are exchanged.

For a satellite close to a resonance ψ_j with mean initial elements

$$(a_0, e_0, i_0, \omega_0, \Omega_0, \lambda_{\odot, 0}),$$

the orbit evolution in the (Ψ, ψ) plane, or equivalently in the (e, ψ) plane if we substitute $\Psi = \sqrt{\mu a(1 - e^2)}/n_1$, is given from the contour line of the implicit equation:

$$H_{\psi_j}(\Psi, \psi; L, \Pi) = H_{\psi_j}(\Psi(a_0, e_0), \psi(\omega_0, \Omega_0, \lambda_{\odot, 0}); L, \Pi),$$

with $L = L(a_0)$, $\Pi = \Pi(a_0, e_0, i_0)$. Notice that Π depends on the resonance j through n_1 and n_2 .

The equations of the motion related the resonant models H_{ψ_j} are

$$\begin{aligned} \frac{d\psi}{dt} &= \frac{\partial H_{\psi_j}}{\partial \Psi}, \\ \frac{d\Psi}{dt} &= -\frac{\partial H_{\psi_j}}{\partial \psi}, \end{aligned} \quad (15)$$

and the associated equilibria are given from the equations

$$\begin{aligned}\frac{d\psi}{dt} &= 0, \\ \frac{d\Psi}{dt} &= 0.\end{aligned}\tag{16}$$

Those stationary solutions of the resonant model represent periodic orbits of the full equations of motion. Their stability is determined from the Hessian eigenvalues of the Hessian of the Hamiltonian \mathcal{H}_{ψ_j} computed at each equilibrium point.

In many applications the equations of motion with respect to the eccentricity are of interest, and thus, by applying the chain rule for the derivatives and using the relations $\Psi = G/n_1$ and $de/dG = -\frac{\sqrt{1-e^2}}{e\sqrt{\mu a}}$ we can derive the semi-canonical form:

$$\begin{aligned}\frac{de}{dt} &= n_1 \frac{\sqrt{1-e^2}}{e\sqrt{\mu a}} \frac{\partial H_{\psi_j}}{\partial \psi} = n_1 \mathcal{C}_{SRP} \frac{\sqrt{1-e^2}}{na} \mathcal{T}_j \sin \psi \\ \frac{d\psi}{dt} &= -n_1 \frac{\sqrt{1-e^2}}{e\sqrt{\mu a}} \frac{\partial H_{\psi_j}}{\partial e} = n_1 \dot{g}_{(J_2, \psi_j)} + n_2 \dot{h}_{(J_2, \psi_j)} + n_3 n_s.\end{aligned}$$

and

$$\begin{aligned}\dot{g}_{(J_2, \psi_j)} &= \dot{g}_{J_2} + \dot{g}_{\psi_j}, \\ \dot{h}_{(J_2, \psi_j)} &= \dot{h}_{J_2} + \dot{h}_{\psi_j},\end{aligned}\tag{17}$$

where $\dot{g}_{J_2}, \dot{h}_{J_2}$ are given in Eq. (9) and

$$\begin{aligned}\dot{h}_{\psi_j} &= \frac{\partial H_{\psi_j, SRP}}{\partial H} = C_{SRP} \frac{e}{na\sqrt{1-e^2} \sin i} \frac{\partial \mathcal{T}_j}{\partial i} \cos \psi, \\ \dot{g}_{\psi_j} &= \frac{\partial H_{\psi_j, SRP}}{\partial G} = C_{SRP} \frac{\sqrt{1-e^2}}{nae} \mathcal{T}_j \cos \psi - \dot{h}_{\psi_j} \cos i,\end{aligned}\tag{18}$$

that is the model developed in [1].

In all the above formulation the angles g, h are not well defined when the eccentricity and/or the inclination are zero. To alleviate this burden we use the modified Delaunay variables in Eq. (10)

$$\begin{aligned}\Lambda &= L, & \lambda &= l + g + h, \\ P &= L - G, & p &= -g - h, \\ Q &= G - H, & q &= -h,\end{aligned}\tag{19}$$

while a unimodular transformation allows to derive a new set of resonant variables (Σ, σ) , similar to the ones introduced in [4] for the case of lunisolar resonances, namely,

$$\begin{aligned}\Sigma &= \frac{P}{k_1}, & \sigma &= k_1 p + k_2 q + k_3 \lambda_\odot, \\ \Phi &= -k_2 P + k_1 Q, & \phi &= \frac{q}{k_1}, \\ \Gamma &= I_s - \frac{k_3 P}{k_1}, & \gamma &= \lambda_\odot.\end{aligned}\tag{20}$$

where k_1, k_2, k_3 are integers appearing in combinations associated to each harmonic in Eq. (4)

j	$\cos \psi_j$	(k_1, k_2, k_3)
1	$\cos(-p - \lambda_\odot)$	$(\mp 1, 0, \mp 1)$
2	$\cos(-p + 2q - \lambda_\odot)$	$(\mp 1, \pm 2, \mp 1)$
3	$\cos(-p + q - \lambda_\odot)$	$(\mp 1, \pm 1, \mp 1)$
4	$\cos(-p + q + \lambda_\odot)$	$(\mp 1, \pm 1, \pm 1)$
5	$\cos(-p + \lambda_\odot)$	$(\mp 1, 0, \pm 1)$
6	$\cos(-p + 2q + \lambda_\odot)$	$(\mp 1, \pm 2, \pm 1)$

(21)

After a Taylor expansion in the resonant action Σ and dropping the constant terms, the resonant Hamiltonian up to a truncation order N takes the form

$$H_{\psi_j}^{(N)} = n_s k_3 \Sigma + C_{J_2} \sum_{n=1}^N c_n \Sigma^n + C_{SRP} \sum_{n=1}^N d_n \Sigma^{n-1/2} \cos \sigma, \quad (22)$$

where c_n, d_n are constant coefficients depending on the dynamical parameters (L, Φ) , the particular resonance (k_1, k_2) and the physical parameters (ε, μ) . We notice that up to second order ($N = 2$) the resonant model is similar to the Second Fundamental Model for first-order in the eccentricity resonances (SFM_I). However, in practice a truncation order of $N \geq 4$ is required to retrieve the qualitative features of the phase space, while higher orders are used for more accurate computations. Actually, the phase-space exploration can be done with the non-truncated resonant Hamiltonian and we retain the complete dynamical portrait of the resonance, a fact that highlights the power of the closed-form averaging process.

Finally, it is common to express the resonant Hamiltonian in terms of Poincaré variables

$$X = \sqrt{2\Sigma} \cos \sigma, \quad Y = \sqrt{2\Sigma} \sin \sigma, \quad (23)$$

with $x = \frac{X}{\sqrt{L}} \sim e \cos \sigma$ and $y = \frac{Y}{\sqrt{L}} \sim e \sin \sigma$ providing a polar representation of the resonant domain, while the truncated Hamiltonian in Eq. (22) takes a polynomial form in x, y coordinates.

4 Bifurcation analysis

From the equations written above it is possible to compute the equilibrium points associated with the dynamical system together with the corresponding stability. The isolated resonance system has two constants of motion (apart from \mathcal{H}): the semi-major is constant due to the averaging and the second integral Π from Eq. (14). The values of Π can be labelled based on the inclination of the corresponding circular orbit $\Pi \equiv \Pi_{circ} = n_1 \cos i_{circ} \sqrt{\mu a} - n_2$. Given a set of values of the dynamical parameters (a, i_{circ}) and the engineering parameter A/m , a phase space is uniquely identified. In this phase space the number

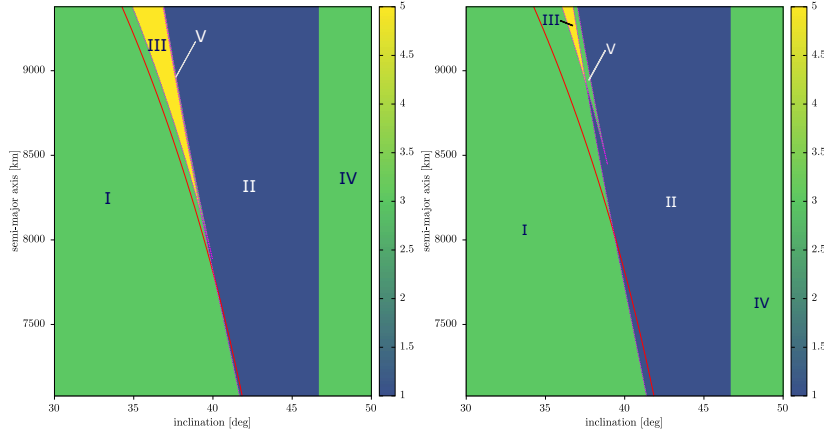


Fig. 2 The bifurcation diagram for resonance ψ_1 . The total number of equilibria, reported in the colorbar, is presented in the dynamical parameter space (a, i_{circ}) . Left: $A/m = 1 \text{ m}^2/\text{kg}$; right: $A/m = 5 \text{ m}^2/\text{kg}$. The red line corresponds to the resonant condition computed from solely the J_2 rate. Inclination stands for inclination of the circular orbit. For the type of equilibria in each region see Tab. 1.

Region	total	$\psi_1 = 0$	$\psi_1 = \pi$
I	3	1 s	1 s & 1 u
II	1	1 s	-
III	5	2 s & 1 u	1 s & 1 u
IV	3	1 s & 1 u	1 s
V	3	2 s & 1 u	-

Table 1 Number of equilibria and their stability (s: stable, u: unstable) for the resonance ψ_1 , corresponding to the five regions of Fig. 2. The corresponding phase space is depicted in Fig. 3.

of equilibrium points and their stability can be defined. By varying the parameters and tracking the structural changes in the system, a bifurcation diagram can be computed. Elliptic and saddle points appear and disappear based on the classical bifurcation theory for 1-DOF systems.

For the two harmonics that dominate in the low Earth orbit region, namely, ψ_1 and ψ_2 [3], in Fig. 2 and in Fig. 4 the possible phase space structures are depicted in the range of semi-major axis $a \in [7000 : 9400]$ km. The black curves define the boundaries of the regions characterized by a different number of equilibrium points and corresponding stability. In red, the curves that would be obtained by considering only the oblateness effect for the rate of precession of ω and Ω are shown, that is, only Eq. (9) instead of Eq. (17).

For the resonant harmonic ψ_1 in Fig. 2 we present two bifurcation diagrams for $A/m = 1 \text{ m}^2/\text{kg}$ (left) and $A/m = 5 \text{ m}^2/\text{kg}$ (right). There are 5 distinct dynamical regions labelled with Latin numbers, defined in Tab. 1, the corresponding phase spaces being shown in Fig. 3.

As just mentioned, the red line corresponds to the resonance location based on the J_2 rates. We observe that for the low $A/m = 1 \text{ m}^2/\text{kg}$ value, this line

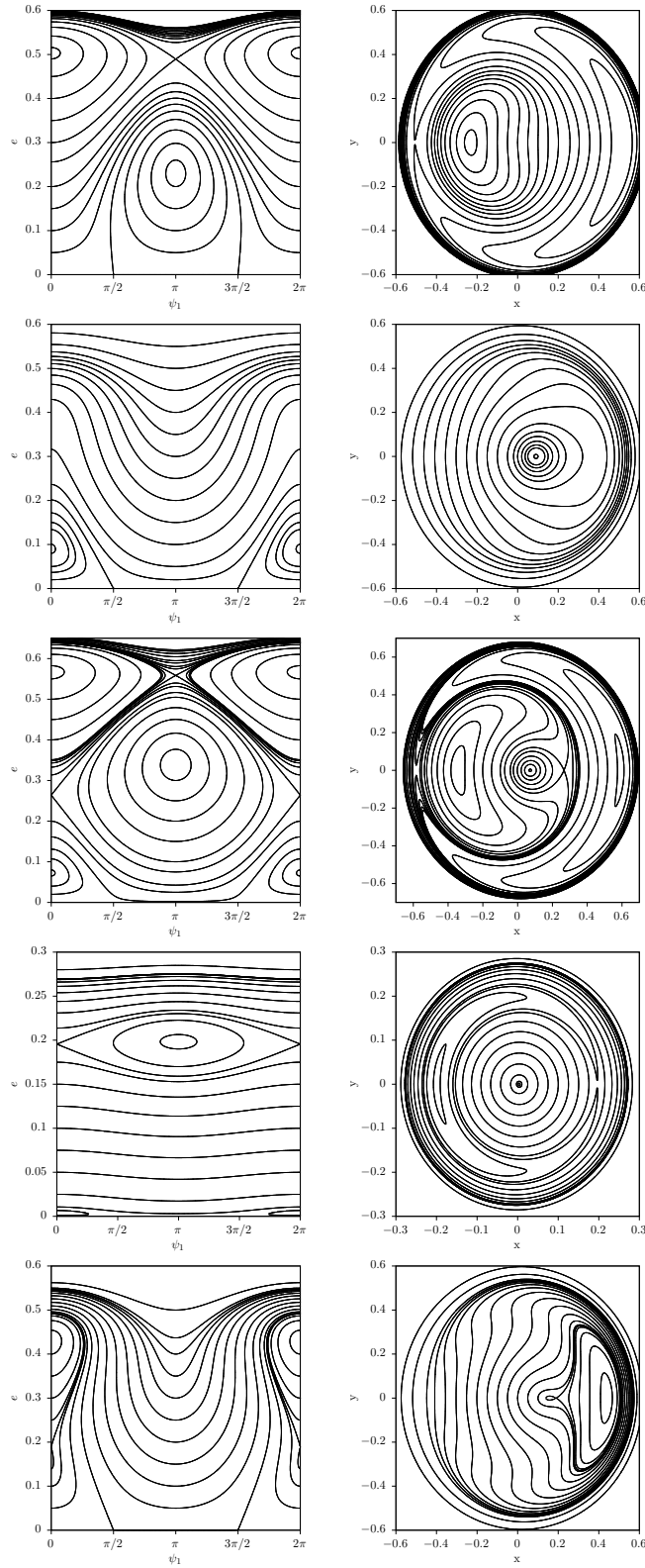


Fig. 3 Resonant phase space portraits for ψ_1 , in $e - \psi$ and $x - y$ variables, according to the regions defined in Tab. 1 (top to bottom).

almost coincides with the transition from region I to region III and from I to II. From Tab. 1 it is easy to see that the following bifurcations take place:

$\psi = 0$:

- transition from region I to region III: saddle-node;
- transition from region V to region II: saddle-node;

$\psi = \pi$:

- transition from region III to region V: saddle-node;
- transition from region I to region II: saddle-node.

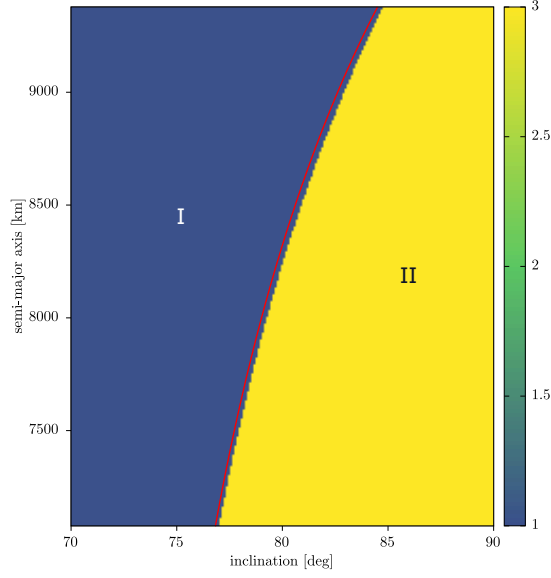


Fig. 4 The bifurcation diagram for resonance ψ_2 assuming $A/m = 1 \text{ m}^2/\text{kg}$. The total number of equilibria, reported in the colorbar, is presented in the dynamical parameter space (a, i_{circ}) . The red line corresponds to the resonant condition computed from solely the J_2 rate. Inclination stands for inclination of the circular orbit. For the type of equilibria in each region see Tab. 2.

Region	total	$\psi_2 = 0$	$\psi_2 = \pi$
I	1	-	1 s
II	3	1 s & 1 u	1 s

Table 2 Number of equilibria and their stability (s: stable, u: unstable) for the resonance ψ_2 , corresponding to the two regions of Fig. 4.

The effect of an increased A/m on the bifurcation diagram is shown in the right panel of Fig. 2. In this case, the exact position of the bifurcation is no longer

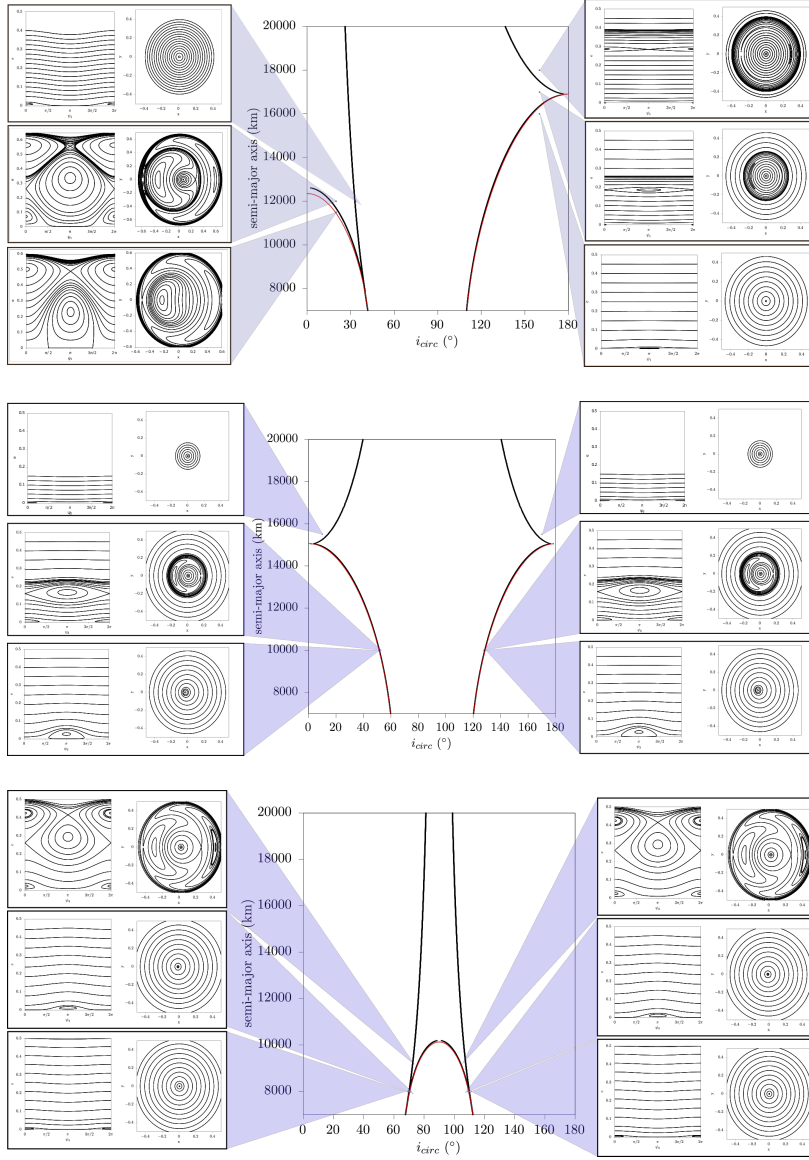


Fig. 5 The bifurcation diagram for resonance ψ_1 (top), ψ_3 (middle) and ψ_4 (bottom). The red curves correspond to the bifurcation that is obtained considering only the oblateness effect in $\dot{\omega}$ and $\dot{\Omega}$.

predicted from the J_2 only rates as significant contributions are added to the $\dot{\omega}$ and $\dot{\Omega}$ rates due to SRP. The number of regions and their structure remains the same, however, the borders between the different regions considerably alter. Specifically, for a fixed i_{circ} the bifurcation for region I to regions II

and III seem to happen at higher altitudes. This is in agreement to previous findings on the planar case ($i_{circ} = 0$) of ψ_1 [12].

A similar analysis is now performed for the resonance ψ_2 . Assuming the same range semi-major axis as in ψ_1 case, we expect this harmonic to dominate in a range of inclinations from $i \in [76 : 84]$. The bifurcation diagram is shown in Fig. 4 and the equilibria with their associated stability are given in Tab. 2. The situation in this case appears to be more straightforward. There are two distinct regions: in region I there exists only 1 stable equilibrium at $\psi_2 = \pi$ while in region II two more equilibria, 1 stable and unstable, appear at $\psi_2 = 0$ after another saddle-node bifurcation. The position of the bifurcation for $A/m = 1 \text{ m}^2/\text{kg}$ is approximately estimated from the J_2 resonant condition (red curve in Fig. 4).

Figure 5 extends the analysis by displaying the bifurcation diagrams for resonances ψ_1 , ψ_3 and ψ_4 , assuming $A/m = 1 \text{ m}^2/\text{kg}$ and a range of semi-major axis $a \in [7000 : 20000]$. As also found in [1], the maximum number of equilibrium points is 5 also for ψ_4 , and it is interesting to note that for ψ_1 it can occur another type of bifurcation apart from the saddle-node: the transcritical one beyond $a \sim 17000 \text{ km}$ and $i_{circ} \in [130^\circ : 150^\circ]$. The bifurcation diagram for ψ_5 and ψ_2 are symmetrical with respect to $i_{circ} = 90^\circ$, the same holds for ψ_6 and ψ_1 .

5 Deorbiting configuration

The phase space analysis can be exploited to compute the initial conditions, in terms of orbital elements and area-to-mass ratio, that can lead to an atmospheric reentry. Since the semi-major axis does not change under the dynamics considered, a natural deorbiting can take place only if the eccentricity increases as much as to attain the critical value $e_{cr} = 1 - r_\oplus/a$.

We consider the case where this condition occurs at either $\psi = 0$ or $\psi = \pi$, meaning that the area-to-mass ratio required is the minimum. Moreover, mindful of the phase space behavior depicted in the previous section (see Fig. 3), the steepest eccentricity growth from a circular orbit takes place starting from $\psi = \pi/2 \vee 3\pi/2$ and following the stable direction associated with a hyperbolic equilibrium point or a libration curve associated with an elliptic equilibrium point. Based on this and following the idea presented in [13] for the planar case, the initial conditions that can enable a natural deorbiting from a circular orbit in the spatial case can be obtained by solving the following equation

$$\mathcal{H}_{\psi_j}(\Psi(e = 0), \psi; L, \Pi) - \mathcal{H}_{\psi_j}(\Psi(e = e_{cr}), \psi; L, \Pi) = 0, \quad \psi = 0 \vee \pi, \quad (24)$$

as a function of C_{SRP} (or, equivalently, A/m). In particular,

$$\begin{aligned} C_{SRP} = \pm \frac{\mu}{6L^{10}n_1^2\mathcal{T}_j\eta_{cr}^5e_{cr}} & \left\{ 4L^9n_1n_3n_s(\eta_{cr} - 1)\eta_{cr}^5 \right. \\ & - \mathcal{C}_{J_2}L^2(n_1^2 - 3n_2^2)\eta_{cr}^2(\eta_{cr}^3 - 1)\mu^3 \\ & \left. + 6\mathcal{C}_{J_2}Ln_2\eta_{cr}(-1 + \eta_{cr}^4)\mu^3\Pi + 3\mathcal{C}_{J_2}(\eta_{cr}^5 - 1)\mu^3\Pi^2 \right\} \end{aligned} \quad (25)$$

where $\eta_{cr} = \sqrt{1 - e_{cr}^2}$, and the coefficients T_j are computed using $c_i = \frac{Ln_2\eta_{cr} + \Pi}{Ln_1\eta_{cr}}$ and $s_i = \sqrt{1 - c_i^2}$. The \pm sign depends on whether the critical eccentricity is attained at $\psi = 0$ or $\psi = \pi$, respectively. Note that only the positive solutions is admissible, because it represents a physical area-to-mass ratio. Moreover, it should be noticed that the solution does not provide any information on the time required to cover the invariant curve up to $e = e_{cr}$.

In the above expression, the only unknown is Π that can be set considering that the deorbiting starts from $e_0 = 0$ and $\psi_0 = \pi/2 \vee 3\pi/2$, following a resonant curve. Given the value of semi-major axis a , the value of the inclination can be found by computing the resonant condition $\dot{\psi} = 0$ at that configuration. Following [1], the resonant condition $\dot{\psi} = 0$ at $\psi = \pi/2 \vee 3\pi/2$ does not depend on the solar radiation pressure, but only on the oblateness effect. In particular, i_0 can be obtained by solving the quadratic equation in $\cos i_0$ [1]

$$c_1 \cos^2 i_0 + c_2 \cos i_0 + c_3 = 0, \quad (26)$$

with

$$c_1 = \frac{15n_2 J_2 r_\oplus^2 n}{4a^2(1 - e^2)^2}; \quad c_2 = -\frac{3n_1 J_2 r_\oplus^2 n}{2a^2(1 - e^2)^2}; \quad c_3 = n_3 n_S - \frac{3n_2 J_2 r_\oplus^2 n}{4a^2(1 - e^2)^2}.$$

5.1 Results

We have applied the procedure just described to the range $a \in [6978 : 15000]$ km, considering a discretization of $\Delta a = 10$ km. The lower limit for the range in a reflects the fact that below about 600 km of altitude a circular orbit decays naturally in 25 years due to the effect of the atmospheric drag.

In Fig. 6, we show the area-to-mass ratio computed by means of Eq. (25), as a function of initial semi-major axis for the six resonant arguments, for prograde orbits. The color reports if the deorbiting occurs at $\psi = 0$ (red) or $\psi = \pi$ (green). It should be noticed that, as already detected numerically [3, 18], the resonant terms $j = 5, 6$ are the least effective ones, requiring very high values of A/m . Moreover, the conditions depicted always correspond to a libration curve.

In Fig. 7, we show, on the left, the value of initial inclination and semi-major axis corresponding to the conditions depicted in Fig. 6 (right). On the right, we show with a thicker point the configurations that actually attain e_{cr} in less than 50 years. The cases where this does not occur are associated to two different behaviors:

- either the dynamics is too slow and this happens, in particular, after the cusps that can be noticed in the figure;
- or there exist two curves, not connected, associated with the same value of \mathcal{H} , for a same integral of motion Λ . This happens, in particular, for $j = 1$ and $j = 4$ before for values of semi-major axis lower than $a = 7500$ km.

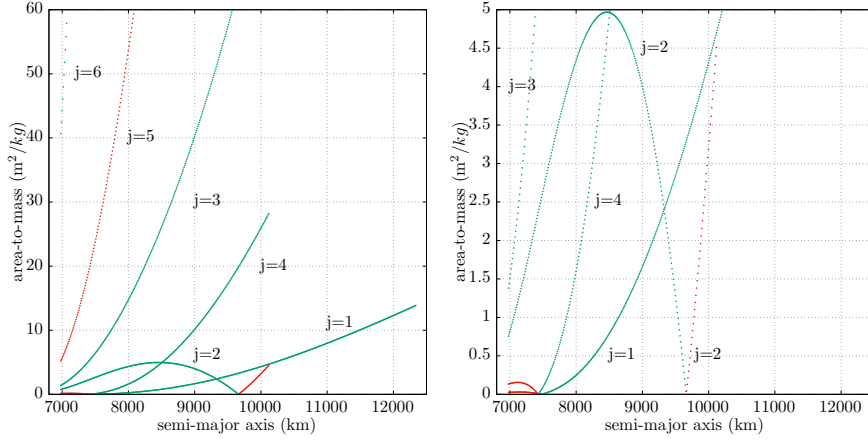


Fig. 6 Minimum area-to-mass ratio required to obtain a natural deorbiting, according to Eq. (25). Red: the deorbiting occurs at $\psi = 0$; green: at $\psi = \pi$. Right: a closer view at feasible values of A/m .

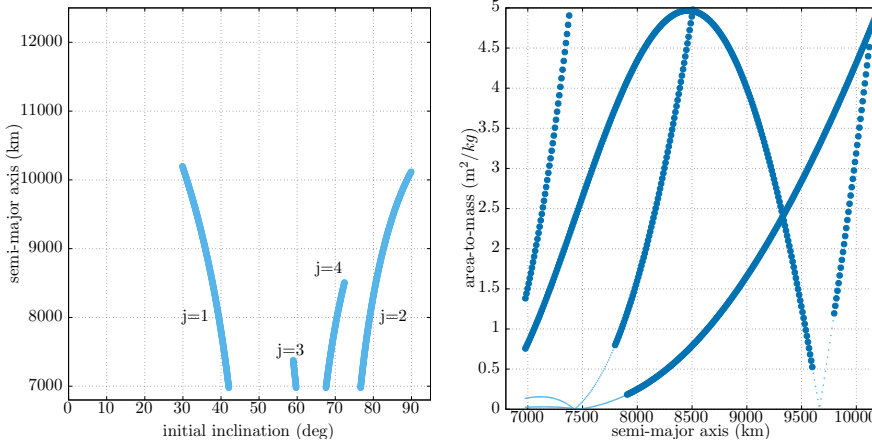


Fig. 7 Left: semi-major axis and inclination for the circular orbits corresponding to the minimum area-to-mass depicted in Fig. 6 on the right. Right: the blue thicker points correspond to the conditions that can deorbit in less than 50 years.

6 Conclusions

In this work, we have extended the analytical development of the equations of motion associated with the coupled oblateness – solar radiation pressure effect. In particular, the Hamiltonian formulation, only partially explained in [2,1] has been here accurately presented. On this basis, the whole phase space in Earth orbit up to $a = 20000$ km has been described by means of a dynamical taxonomy, that shows where the main bifurcations occurs, in particular the saddle-node and the transcritical ones. Finally, the analytical value of the area-to-mass ratio required to de-orbit has been provided, for the first time in

the three-dimensional case, and the corresponding applications for a feasible disposal strategy by means of a solar sail has been presented.

Acknowledgements Part of the research leading to these results has received funding from the European Research Council (ERC) under the European Union’s Horizon 2020 research and innovation programme as part of project COMPASS (Grant agreement No. 679086).

Compliances with ethical standards

Conflict of Interest Statement On behalf of all authors, the corresponding author states that there is no conflict of interest.

References

1. Alessi, E.M., Colombo, C., Rossi, A.: Phase space description of the dynamics due to the coupled effect of the planetary oblateness and the solar radiation pressure perturbations. *Celestial Mechanics and Dynamical Astronomy* **131**, 43 (2019). DOI 10.1007/s10569-019-9919-z
2. Alessi, E.M., Schettino, G., Rossi, A.: Solar radiation pressure resonances in low earth orbits. *Monthly Notices of the Royal Astronomical Society* **473**, 2407–2414 (2018). DOI 10.1093/mnras/stx2507
3. Alessi, E.M., Schettino, G., Rossi, A., Valsecchi, G.B.: Natural highways for end-of-life solutions in the LEO region. *Celestial Mechanics and Dynamical Astronomy* **130**, 34 (2018). DOI 10.1007/s10569-018-9822-z
4. Breiter, S.: Lunisolar Resonances Revisited. *Celestial Mechanics and Dynamical Astronomy* **81**, 81–91 (2001)
5. Cook, G.E.: Luni-Solar Perturbations of the Orbit of an Earth Satellite. *Geophysical Journal* **6**, 271–291 (1962). DOI 10.1111/j.1365-246X.1962.tb00351.x
6. Deprit, A.: Canonical transformations depending on a small parameter. *Celestial Mechanics* **1**(1), 12–30 (1969). DOI 10.1007/BF01230629
7. Hori, G.: Theory of General Perturbation with Unspecified Canonical Variable. *Publications of the Astronomical Society of Japan* **18**, 287 (1966)
8. Kaula, W.M.: Development of the lunar and solar disturbing functions for a close satellite. *Astronomical Journal* **67**(5), 300–303 (1962). DOI 10.1086/108729
9. Kozai, Y.: Secular perturbations of asteroids with high inclination and eccentricity. *The Astronomical Journal* **67**, 591 (1962). DOI 10.1086/108790
10. Krivov, V.A., Getino, J.: Orbital evolution of high-altitude balloon satellites. *Astronomy and Astrophysics* **318**, 308–314 (1997)
11. Lidov, M.L.: The evolution of orbits of artificial satellites of planets under the action of gravitational perturbations of external bodies. *Planetary Space Science* **9**, 719–759 (1962). DOI 10.1016/0032-0633(62)90129-0
12. Lücking, C., Colombo, C., McInnes, C.R.: A passive satellite deorbiting strategy for medium earth orbit using solar radiation pressure and the j_2 effect. *Acta Astronautica* **77**, 197–206 (2012). DOI 10.1016/j.actaastro.2012.03.026
13. Lücking, C., Colombo, C., McInnes, C.R.: Solar radiation pressure-augmented deorbiting: Passive end-of-life disposal from high-altitude orbits. *Journal of Spacecraft and Rockets* **50**(6), 1256–1267 (2013). DOI 10.2514/1.A32478
14. Mignard, F., Henon, M.: About an unsuspected integrable problem. *Celestial Mechanics* **33**, 239–250 (1984). DOI 10.1007/BF01230506
15. Musen, P.: The influence of the solar radiation pressure on the motion of an artificial satellite. *Journal of Geophysical Research* **65**(5), 1391–1396 (1960). DOI 10.1029/JZ065i005p01391

16. Musen, P., Bryant, R., Bailie, A.: Perturbations in perigee height of vanguard i. *Science* **131**(3404), 935–9366 (1960). DOI 10.1126/science.131.3404.935
17. Oyama, T., Yamakawa, H., Omura, Y.: Orbital dynamics of solar sails for geomagnetic tail exploration. *Journal of Guidance Control and Dynamics* **45**(2), 316–323 (2008). DOI 10.2514/1.31274
18. Schaus, V., Alessi, E.M., Schettino, G., Rossi, A., Stoll, E.: On the practical exploitation of perturbative effects in low Earth orbit for space debris mitigation. *Advances in Space Research* **63**, 1979–1991 (2019). DOI 10.1016/j.asr.2019.01.020
19. Scheeres, D.J.: Orbit mechanics about asteroids and comets. *Journal of Guidance Control and Dynamics* **35**(3), 987–997 (2012). DOI 10.2514/1.57247
20. Shapiro, I.I., Jones, H.M.: Perturbations of the orbit of the echo balloon. *Science* **132**(3438), 1484–1486 (1960). DOI 10.1126/science.132.3438.1484